Journal of Materials Chemistry A

PAPER

View Article Online
View Journal | View Issue



Cite this: J. Mater. Chem. A, 2016, 4, 4516

# Pt/C–$LiCoO_2$ composites with ultralow Pt loadings as synergistic bifunctional electrocatalysts for oxygen reduction and evolution reactions†

Chao Su,[a] Tao Yang,[b] Wei Zhou,[c] Wei Wang,[a] Xiaomin Xu[c] and Zongping Shao*[ad]

Received 21st December 2015
Accepted 17th February 2016

DOI: 10.1039/c5ta10492k

www.rsc.org/MaterialsA

Oxygen reduction and evolution reactions (ORR and OER) are of prime importance for many energy conversion and storage devices, such as regenerative fuel cells and rechargeable metal–air batteries. However, the sluggish kinetics of the ORR and OER strongly limit the efficiency and performance of these electrochemical systems and jeopardize the route of commercialization. Therefore, the design and development of bifunctional electrocatalysts with high activity for both the ORR and OER is challenging but urgent and crucial. Here, we took advantage of Pt/C and $LiCoO_2$ with outstanding ORR activity and high intrinsic OER activity, respectively, to develop a composite material with ultralow Pt loading as a bifunctional catalyst for the ORR and OER in alkaline media. This catalyst was fabricated *via* simple ultrasonic mixing, exhibiting superb electrocatalytic activity and good stability. Its ORR activity is comparable to that of the commercial Pt/C catalyst and its OER activity is better than that of single $LiCoO_2$, owing to the synergetic effect between Pt and $LiCoO_2$, which has been demonstrated through the X-ray photoelectron spectroscopy (XPS) characterisation technique. Remarkably, surprisingly high ORR mass activity (2.04 A $mg_{Pt}^{-1}$ at 0.8 V *vs.* RHE) and enhanced bifunctionality ($\Delta E$ = 0.91 V) were obtained for the Pt–$LiCoO_2$ composite catalyst with a mass ratio of 1 : 49 for Pt/$LiCoO_2$. Our work opens up a new track to exploit highly efficient catalysts with reduced consumption of Pt, meanwhile maintaining the optimal catalytic activity and durability.

## Introduction

Increasing energy demands and critical issues of climate change and environmental protection have prompted considerable research interest in exploring renewable and clean electrochemical energy conversion and storage systems with high efficiency and low cost.[1,2] To this end, rechargeable metal–air batteries and regenerative fuel cells have received tremendous attention because of their advantages of extremely high energy density and environmental benignity.[3–5] These electrochemical energy systems are highly attractive for electrified transportation, and smart grid and stationary power sources, which may help us to build up a low-carbon and low-emission sustainable future. Both the oxygen reduction reaction (ORR) and oxygen evolution reaction (OER) are involved in such energy technologies, which play significant roles equally. However, the kinetically sluggish ORR and OER have become the current bottleneck of these energy devices, and largely precluded their large-scale commercial application.[6–9] Although intensive and extensive research efforts have been made during the past decades,[10–13] it is still very challenging to search for more active and stable electrocatalysts, especially for highly efficient catalysts with dual functionality for aforementioned reactions.

So far, noble metal catalysts such as Pt or Pt alloys have been widely used as oxygen catalysts for the ORR with a desirable performance in low-temperature fuel cells because of their ideal electrocatalytic activities.[14–17] However, Pt is known to be expensive and rare in the earth, hindering its practical application; therefore, great efforts have been directed towards the development of alternative low-Pt-loading catalysts, enabling competitiveness economically. The electrode activity for the OER is another big challenge for regenerative fuel cells and rechargeable metal–air batteries, besides the rate-determining step of the ORR over the electrode in fuel cells. Noble metal oxides (*e.g.*, $IrO_2$ and $RuO_2$) are generally applied to meet the requirements of fast kinetics and low overpotentials for the OER,[18,19] but still they cannot circumvent the issue of high-price and scarcity found with Pt. It is urgent to develop new types of

[a]Department of Chemical Engineering, Curtin University, Perth, WA 6845, Australia. E-mail: zongping.shao@curtin.edu.au; Tel: +61 8 9266 4702
[b]Centre of Mechanical Technology and Automation (TEMA), Department of Mechanical Engineering, University of Aveiro, 3810-193, Aveiro, Portugal
[c]State Key Laboratory of Materials-Oriented Chemical Engineering, College of Chemistry and Chemical Engineering, Nanjing Tech University, No. 5 Xin Mofan Road, Nanjing 210009, P. R. China
[d]State Key Laboratory of Materials-Oriented Chemical Engineering, College of Energy, Nanjing Tech University, No. 5 Xin Mofan Road, Nanjing 210009, P. R. China. E-mail: shaozp@njtech.edu.cn

† Electronic supplementary information (ESI) available. See DOI: 10.1039/c5ta10492k

low-cost but active catalysts for electrocatalytic evolution of oxygen. Along with the intensive research in this scope, many transition metal oxides have been studied as OER electrocatalysts in recent years, such as single-phase oxide, perovskite-type and spinel-type catalysts.[20–27] $LiCoO_2$, one of the most well-known cathode materials for lithium-ion batteries,[28] has recently been proved to be an excellent electrocatalyst for the OER in alkaline media.[29–34] Furthermore, when $LiCoO_2$ was chemically delithiated to form $Li_{1-x}CoO_2$ or developed with some particular microstructure (*e.g.* nanostructure),[33,34] it also exhibited a high ORR activity. However, the preparation methods and techniques are usually quite complex and sophisticated. Therefore, the development of bifunctional electrocatalysts with highly effective catalytic activities for both the ORR and OER *via* a facile synthesis is imperative to realize large-scale commercialization of regenerative fuel cells and rechargeable metal–air batteries.

Lately, metal oxide supported Pt particles have been used to attempt effective composite catalysts. The obtained catalysts displayed enhanced activity and stability towards the ORR/OER. They mainly utilize the synergetic "spillover" effects between platinum and the support to influence the adsorption/desorption behavior of intermediate species at the catalyst surfaces and altered the electronic structure of platinum, hence promoting the rate determining steps in the corresponding reactions.[35–38] Remarkably, a great amount of experimental results have shown that the combination of different types of electrocatalysts to form composite electrodes could result in improved catalytic activity for the ORR and OER, much better than each of the individual components.[39–45] It is promising to develop bi-functional electrocatalysts with enhanced activity for both the ORR and OER taking advantage of the synergic effects. Although the ORR and OER mechanisms are complicated, attributed to the multiple reaction steps, the formation of composite electrodes could effectively improve the reaction kinetics due to the synergistic effect of each component for the rate limiting step(s). Previously, we have successfully demonstrated a composite of Pt/C (known for its high activity for the ORR) and perovskite-type $Ba_{0.5}Sr_{0.5}Co_{0.8}Fe_{0.2}O_{3-\delta}$ (BSCF) oxide (known for its high activity for the OER). The catalytic activity for the ORR and OER in alkaline media was obviously improved compared with the condition of the absence of each other, suggesting the existence of synergistic effects amongst Pt/C and BSCF.[45] However, the Pt content in this reported composite is still very high, with a value of at least 20 wt%, which has to be reduced in the electrocatalyst. It is of crucial importance to bring these electrochemical technologies to a competitive commercial position.

In this study, we extended this universal and facile strategy to develop a composite material with Pt/C and $LiCoO_2$ as the bifunctional electrocatalyst for the ORR and OER in alkaline media for the first time. It should be noted that the Pt loading in the as-prepared composite has been reduced to an ultralow level of 2 wt%. To the best of our knowledge, until now, the lowest Pt content in low-Pt-loading catalyst systems has been realized through our attempt and efforts. The composite catalysts delivered superb ORR catalytic activity comparable with that of commercial Pt/C alone, as well as more excellent performance for the OER process than that of $LiCoO_2$ alone. Our study demonstrated that the Pt/C–$LiCoO_2$ composite material is a promising candidate as a bifunctional oxygen catalytic electrode material for rechargeable metal–air batteries and regenerative fuel cell devices.

# Experimental

### Synthesis and physicochemical characterization

$LiCoO_2$ was synthesized by a traditional solid-state reaction method reported previously.[33] Stoichiometric amounts of $Li_2CO_3$ (Sigma-Aldrich) and $Co_3O_4$ (Sigma-Aldrich) were ground and mixed thoroughly using high energy ball milling (Fritsch Pulverisette 6) in absolute ethanol at 400 rpm for 1 h, followed by drying and sintering at 800 °C for 5 h in air. Platinum on carbon, Pt/C, with a Pt loading of 20 wt% was used in this study, which was purchased from Sigma-Aldrich. The samples were characterized by X-ray diffraction (XRD, Rigaku Smartlab 3 kW) using filtered Cu K$\alpha$ radiation ($\lambda$ = 1.5406 Å) in a step-scan mode within the $2\theta$ range of 10–90° at 0.02° per step. X-ray photoelectron spectroscopy (XPS) analysis was conducted on a Kratos AXIS Ultra DLD system under UHV conditions with an Al K$\alpha$ X-ray, and the data were analyzed using the Kratos Vision and CasaXPS software, with the cross-calibration to C 1s = 284.8 eV. The morphology of the catalysts was investigated by transmission electron microscopy (TEM, JEOL 2100).

### Electrode preparation

Three kinds of Pt–$LiCoO_2$ composite electrocatalysts with different mass ratios of Pt to $LiCoO_2$ (1 : 9, 1 : 19 and 1 : 49) were prepared and studied. In order to compare with the commercial Pt/C electrocatalyst (20 wt% loading), the same mass ratios of catalyst to carbon (2 : 8) were chosen for all the Pt–$LiCoO_2$ composite and single $LiCoO_2$ electrocatalysts. Taking Pt–$LiCoO_2$ (1 : 9) as an example, 1 mg of Pt/C (20 wt% loading), 1.8 mg of $LiCoO_2$ and 7.2 mg of carbon black (Super P, Alfa Aesar) were ultrasonically mixed in a solution containing 1 ml of absolute ethanol and 0.1 ml of Nafion solution (5 wt% in isopropanol and water solution) for 2 h, forming a catalyst ink with a concentration of ~1.818 $mg_{catalyst}$ $mL^{-1}$. Next, 7 μL of the catalyst ink was pipetted onto the surface of a glassy carbon rotating disk electrode (GC-RDE, 0.196 $cm^2$, Pine Research Instrumentation, USA) or a rotating ring-disk electrode (RRDE, GC disk with a 320 μm gap Pt ring, Pine Research Instrumentation, USA) and dried in air, yielding a catalyst loading of ~0.0649 mg $cm^{-2}_{disk}$. Before coating the catalyst, the RDE or RRDE was polished with 0.05 μm and/or 0.3 μm of $Al_2O_3$ slurry, and rinsed with ethanol and ultrapure water.

### Electrochemical measurements

All the electrochemical measurements were conducted in a three-electrode glass cell (Pine Research Instrumentation, USA) using a CHI 760E bipotentiostat (CH Instruments, Inc., USA). The electrolyte was 0.1 M KOH solution. The catalyst-coated RDE or RRDE was employed as the working electrode,

a platinum wire as the courter electrode, and an Ag/AgCl (4 M KCl filled) electrode as the reference electrode. All the potential values mentioned in this study were referenced to that of the reversible hydrogen electrode (RHE) with the relation of $E$(RHE) = $E$(Ag/AgCl) + 0.948 V, according to the calibration measurement in $H_2$-saturated 0.1 M KOH electrolyte with two platinum wires as working and counter electrodes by measuring hydrogen oxidation/evolution currents on the working electrode. Cyclic voltammograms (CVs) were carried out at a scan rate of 50 mV $s^{-1}$ in an $O_2$-saturated electrolyte. Linear sweep voltammograms (LSVs) were recorded at a scan rate of 5 mV $s^{-1}$ in the $O_2$-saturated electrolyte from 1.148 to 0.348 V (ORR) with varying rotating speeds (2400, 2000, 1600, 1200, 800 and 400 rpm) or from 1.148 to 1.948 V (OER) at 1600 rpm. The kinetic parameters for the ORR were calculated by the Koutecky–Levich equation:

$$\frac{1}{J} = \frac{1}{J_K} + \frac{1}{J_L} = \frac{1}{J_K} + \frac{1}{B\omega^{0.5}} \quad (1)$$

$$B = 0.62nFC_oD_o^{2/3}\upsilon^{-1/6} \quad (2)$$

where $J$ is the measured current density, $J_K$ and $J_L$ correspond to the kinetic and diffusion-limiting current densities, $\omega$ is the electrode rotating rate (rad $s^{-1}$), $n$ is the electron transfer number, $F$ is the Faraday constant, $C_o$ is the bulk concentration of $O_2$ in the electrolyte, $D_o$ is the diffusion coefficient of $O_2$, and $\upsilon$ is the kinetic viscosity of the electrolyte.

RRDE voltammograms for the ORR were obtained at a scan rate of 5 mV $s^{-1}$ from 1.148 to 0.348 V (disk electrode) at different rotating rates in the $O_2$-saturated electrolyte. The ring potent was a constant value of 1.448 V, which is considered to be sufficiently high to oxidize any $HO_2^-$ intermediate.[46,47] The electron transfer number ($n$) and the production percentage of the $HO_2^-$ intermediate were determined using the following equations:

$$n = 4 \times \frac{I_d}{I_d + I_r/N} \quad (3)$$

$$\%\ HO_2^- = 100 \times \frac{2I_r/N}{I_d + I_r/N} \quad (4)$$

where $I_d$ and $I_r$ are the disk and ring current, respectively, and $N$ is the current collection efficiency of the Pt ring (here, $N = 0.37$).

## Results and discussion

### Bulk and surface structures

Fig. 1a shows the room-temperature XRD patterns of the Pt–$LiCoO_2$ composites with different mass ratios of Pt to $LiCoO_2$ fabricated by simple ultrasonic mixing, and the pristine $LiCoO_2$ synthesized through high-temperature calcination at 800 °C and commercial Pt/C were also provided as the reference. Impurity phases in the obtained $LiCoO_2$ sample were not detected, indicating the formation of pure single-phase $LiCoO_2$. All the diffraction peaks can be well indexed to a layered $\alpha$-$NaFeO_2$ structure with the $R\bar{3}m$ space group. This well-known structure consists of alternating planes of coordinated Li and Co ions, which are separated by close-packed oxygen layers.[48,49] According to Rietveld refinement of the XRD data, the lattice parameters were found to be $a = b = 2.817(6)$ Å and $c = 14.05(8)$ Å ($c/a$ = 4.988), which were in alignment with the literature results,[48–50] and further suggested a well-formed layered structure of $LiCoO_2$. The XRD of commercial Pt/C presents broad diffraction peaks, indicating the nanoscale crystalline characteristic of the Pt particles. It is in good accordance with the ~3 nm Pt particles in the commercial Pt/C (TEM image in Fig. S1†). After forming the composites with $LiCoO_2$, the intensity of Pt diffraction peaks dropped to a very low level that only the main peak at the 2$\theta$ of 39.8° was observed, which could be attributed to the small amount of Pt in the composite catalysts. For the $LiCoO_2$ in the three composites, very similar lattice parameters as well as the values of $c/a$ to the pristine $LiCoO_2$ were obtained, which were $a = b = 2.816(2)$ Å, $c = 14.05(0)$ Å, $c/a = 4.989$ for Pt–$LiCoO_2$ (1 : 9), $a = b = 2.817(2)$ Å, $c = 14.05(3)$ Å, $c/a = 4.988$ for Pt–$LiCoO_2$ (1 : 19), and $a = b = 2.816(7)$ Å, $c = 14.05(2)$ Å, $c/a$ = 4.989 for Pt–$LiCoO_2$ (1 : 49). The results suggest that the phase structure of the $LiCoO_2$ cannot be affected after the introduction of Pt/C.

The XRD patterns are very similar to one another, which only reveal the bulk composition information. Therefore, more information on the surface of the as-prepared catalysts was

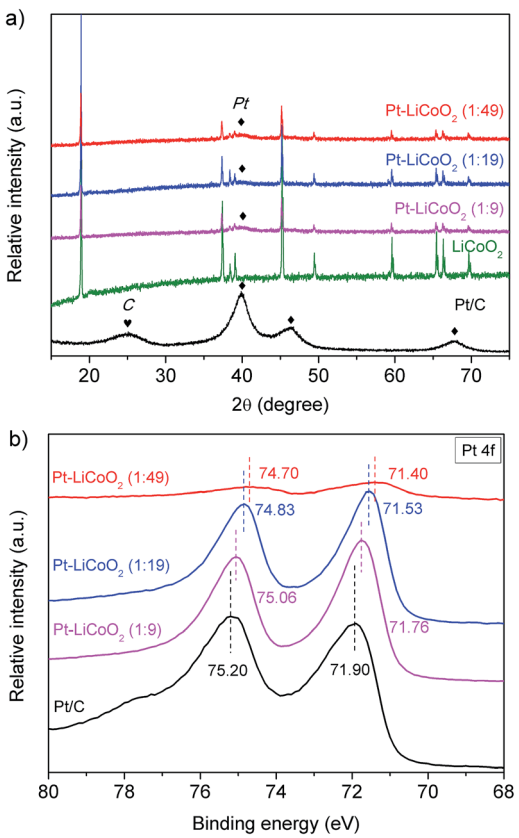


Fig. 1 (a) Powder XRD patterns and (b) Pt 4f XPS spectra of Pt/C, $LiCoO_2$ and the as-prepared Pt–$LiCoO_2$ composites with different mass ratios.

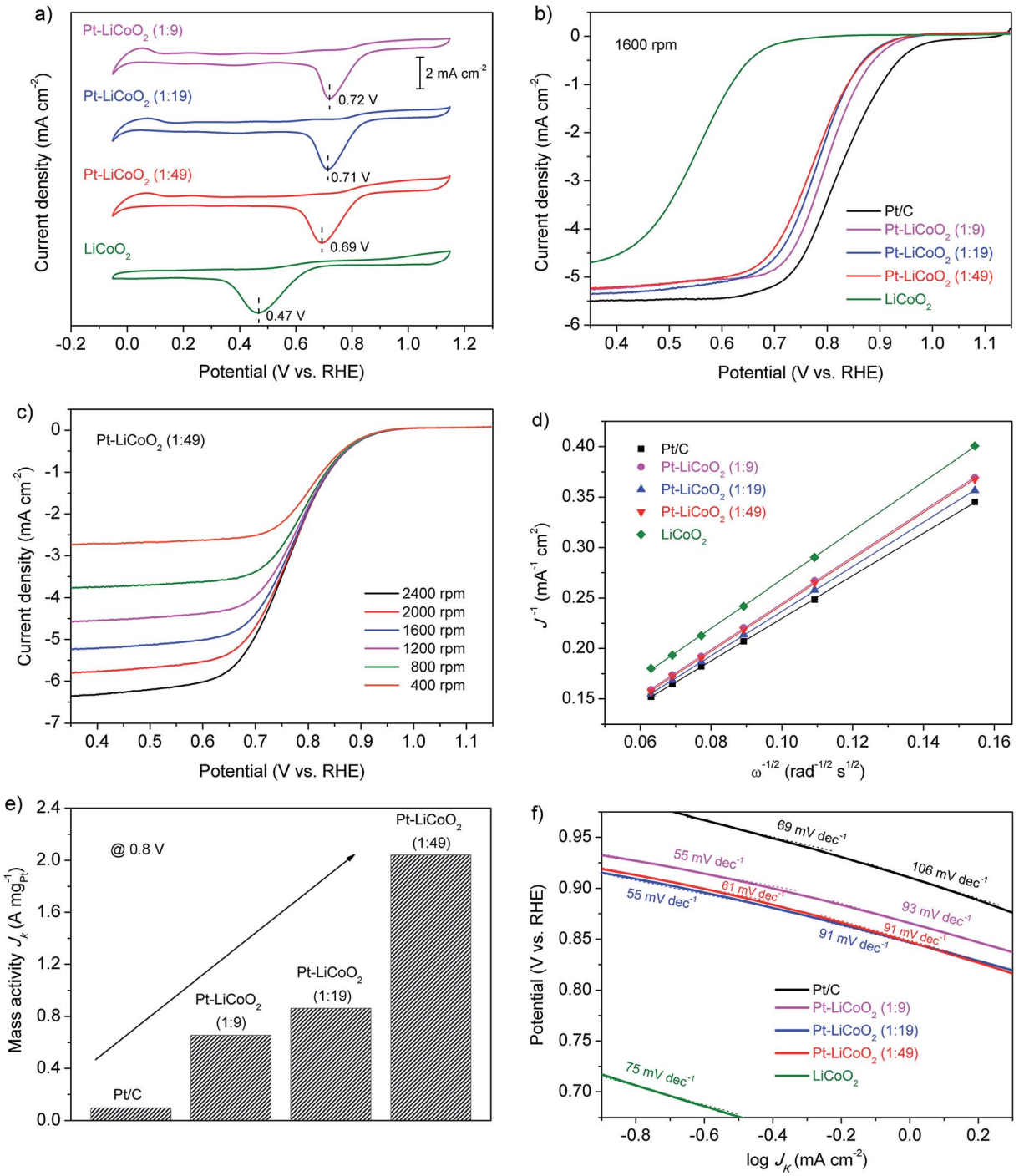


Fig. 2 (a) CV curves of the ORR on $LiCoO_2$ and the as-prepared Pt–$LiCoO_2$ composites with different mass ratios in an $O_2$-saturated 0.1 M KOH solution at a scan rate of 50 mV $s^{-1}$. (b) LSV curves of various electrocatalysts on the RDE at 1600 rpm in an $O_2$-saturated 0.1 M KOH solution at a scan rate of 5 mV $s^{-1}$. (c) LSV curves of Pt–$LiCoO_2$ (1 : 49) on RDE at different rotating rates. (d) K–L plots at 0.35 V for various electrocatalysts on the basis of the RDE data in (c) and Fig. S4 of the ESI.† (e) ORR mass activity of various catalysts at 0.8 V. (f) Tafel plots based on the LSV curves in (b).

collected from the XPS characterization. As shown in Fig. 1b, typical characteristic peaks of Pt $4f_{7/2}$ and Pt $4f_{5/2}$ were observed at binding energies (BEs) of 71.90 and 75.20 eV, respectively for the commercial Pt/C. In the case of Pt–$LiCoO_2$ composites, the spectra of Pt 4f shifted to a lower BE with the reduction of the Pt content in the composites, a similar phenomenon was also observed by Zhu *et al.*[45] It suggests that the electronic structure of Pt was probably modified through the interaction between Pt and $LiCoO_2$. In addition, Co 2p and O 1s XPS spectra of the electrocatalysts are also given in Fig. S2 of the ESI.† All the

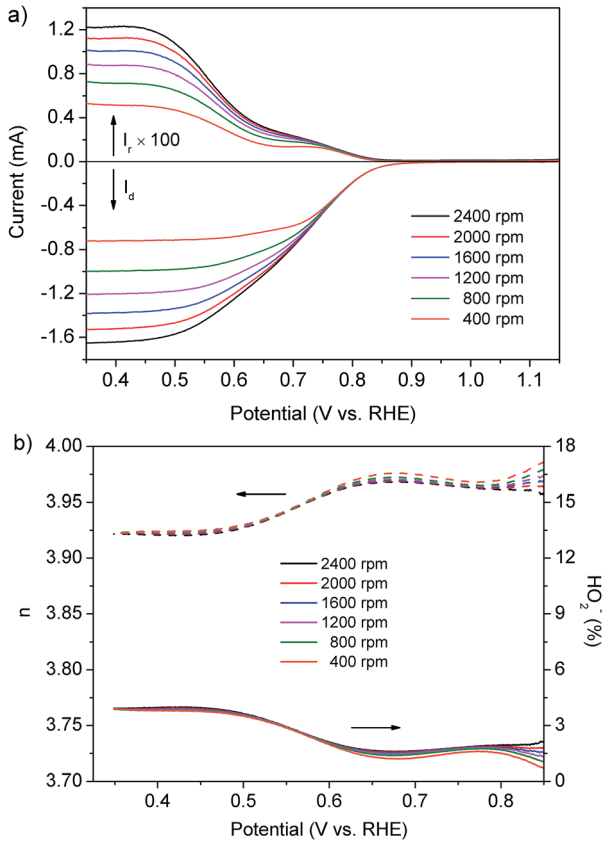


Fig. 3 (a) Disk (bottom) and ring currents (top, multiplied by 100) of the Pt–$LiCoO_2$ (1 : 49) catalyst collected on the RRDE at different rotating rates in $O_2$-saturated 0.1 M KOH electrolyte. (b) The electron transfer number (*n*, dash line) and percentage of $HO_2^-$ (solid line) of the Pt–$LiCoO_2$ (1 : 49) catalyst at various potentials based on the RRDE data in (a).

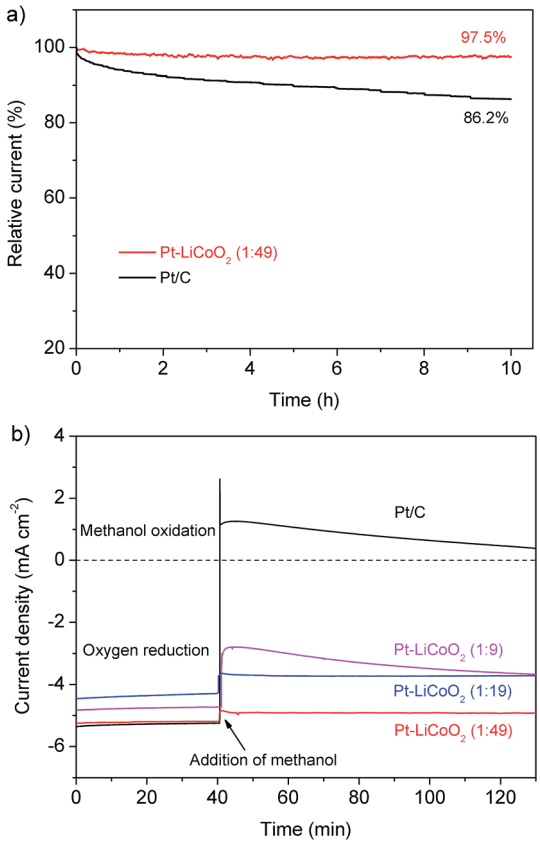


Fig. 4 (a) Current–time chronoamperometric responses of Pt–$LiCoO_2$ (1 : 49) and Pt/C catalysts supported on the RDE (1600 rpm) at 0.65 V. (b) Chronoamperometric responses of various electrocatalysts supported on the RDE (1600 rpm) at 0.65 V in $O_2$-saturated 0.1 M KOH electrolyte without methanol (0–40 min) and with 1 M methanol (40–130 min).

catalysts show a Co $2p_{3/2}$ main peak at around 780 eV with a satellite peak at 790 eV and a Co $2p_{1/2}$ main peak at around 795 eV with a satellite peak at 805 eV, which demonstrates that the oxidation state is $Co^{3+}$ in the $LiCoO_2$ and Pt–$LiCoO_2$ composites.[49,51] According to the investigation of Dahéron *et al.*, there was no $Co^{2+}$ in these samples because the strong broadening of the main peak and very intense satellite peaks at 786 eV (Co $2p_{3/2}$) and 803 eV (Co $2p_{1/2}$) related to the characterization of $Co^{2+}$ coordinated by oxygen are not detected here.[51] For the Pt–$LiCoO_2$ (1–9) sample, the core peaks of Co 2p slightly shifted to higher BEs compared to the pristine $LiCoO_2$, indicating possible partial oxidation of surface $Co^{3+}$ to $Co^{4+}$, and it has been reported that the presence of $Co^{4+}$ could facilitate the OER.[52,53] The XPS spectra of O 1s displayed two peaks at BEs of around 529.5 and 531.4 eV for all the samples, which correspond to the lattice oxygen and adsorbed species at the surface. Compared with the pristine $LiCoO_2$, the ratio of peak intensities of surface to lattice oxygen increased with the increase of Pt content in the composites. It means that a stronger interaction existed between the composite catalysts and adsorbed oxygen-containing species due to the synergistic effect, which is beneficial for the process of the ORR.

## Electrochemical behaviour for the ORR

To evaluate the electrocatalytic activity of the obtained composite catalysts with different compositions for the ORR, CVs tests were first conducted in $O_2$-saturated 0.1 M KOH solution. It was also compared with that of pristine $LiCoO_2$ and commercial Pt/C (Fig. S3†). As shown in Fig. 2a & S3 of the ESI,† all the detected samples presented distinct single oxygen reduction peaks, suggesting the conspicuous catalytic activity for the ORR. The shape of CV curves for all the composite catalysts was more similar to that of $LiCoO_2$ than that of Pt/C, because the proportion of $LiCoO_2$ in the composites was larger. However, the ORR peaks of the composite catalysts appeared at around 0.71 V, which shifted greatly to positive potentials compared with that of $LiCoO_2$ with a value of 0.47 V, and were very close to the cathodic peak of Pt/C (0.81 V), indicating the excellent electrocatalytic activity towards the ORR. Similar trends were further verified by the RDE measurements. Fig. 2b shows a comparison of LSV curves for each of the catalysts performed at 1600 rpm. The ORR on the pristine $LiCoO_2$ electrode initiated at around 0.70 V, and then a continuous increase in the current density was witnessed without an obvious current plateau. All the prepared Pt–$LiCoO_2$ composite

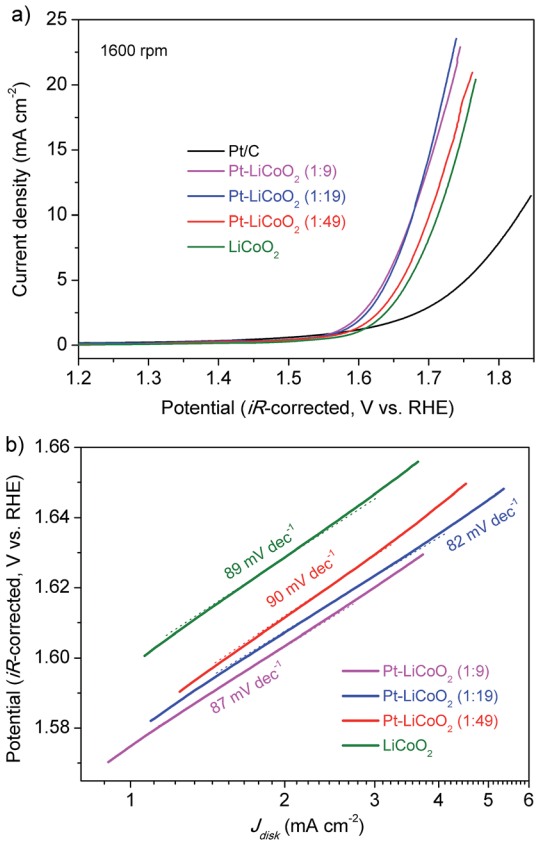


Fig. 5 (a) LSV curves and (b) corresponding Tafel plots of the various electrocatalysts on the RDE at 1600 rpm in $O_2$-saturated 0.1 M KOH electrolyte at a scan rate of 5 mV s$^{-1}$.

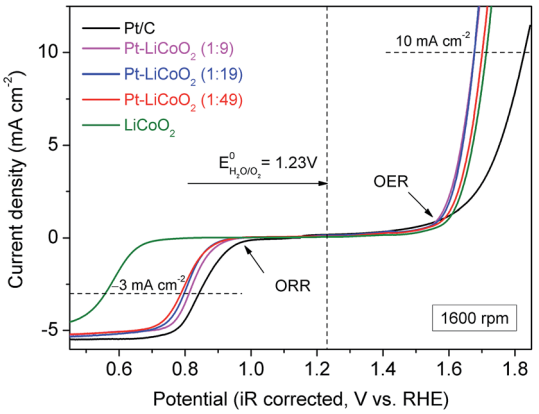


Fig. 6 Oxygen electrode activities of electrocatalysts within the potential window of the ORR and OER on the RDE in $O_2$-saturated 0.1 M KOH electrolyte.

catalysts displayed similar potentials for the commencement of the ORR (~0.96 V), which were more positive than that of the $LiCoO_2$ electrode, and much closer to that of commercial Pt/C (~1.0 V), indicating a more facile ORR process. The wide current plateau on all the Pt–$LiCoO_2$ composites is considered as the strong limiting diffusion current and suggests a diffusion-dominated process that is related to a favourable four-electron ORR pathway, as is also observed on the Pt/C catalyst. Additionally, as compared with a half-wave potential of 0.554 V obtained from the $LiCoO_2$ electrode, the half-wave potentials significantly shifted to 0.799, 0.781 and 0.775 V, positively, for Pt–$LiCoO_2$ (1 : 9, 1 : 19 and 1 : 49) composites, respectively, which are only approximately 0.05 V more negative than that of Pt/C (0.825 V). Furthermore, Pt–$LiCoO_2$ composite catalysts presented a comparable limiting current density with that observed on Pt/C at 0.35 V, even for the sample with the Pt content of only 2 wt%, which is 1.14 times that of the pristine $LiCoO_2$ electrode. All of the above results evidence that the ORR catalytic activity of obtained composites was greatly enhanced by the synergistic effect between Pt and $LiCoO_2$.

A more detailed study of the RDE measurements at rotating rates from 400 to 2400 rpm was conducted, allowing further insight into the ORR kinetics and electrocatalytic processes on the aforementioned catalysts (Fig. 2c and S4 of the ESI†). Fig. 2d shows the K–L plots of various catalysts constructed from rotation rate dependent current density. The linearity of the K–L plots indicates first-order reaction kinetics towards the concentration of dissolved oxygen, and near parallelism of the fitting lines, especially for the composite catalysts and Pt/C, suggests an efficient four-electron-dominated ORR pathway on all of the catalysts. Considering the catalysts' cost and the economic feasibility, the ORR mass activity on the basis of the Pt content of the as-prepared composite catalysts is calculated, which can reflect the ORR intrinsic activity of catalysts.[54] The kinetic currents at a potential of 0.8 V were used to determine the activities. As shown in Fig. 2e, a significant improvement in mass activity was observed for the Pt–$LiCoO_2$ (1 : 49) catalyst (2.04 A $mg_{Pt}^{-1}$) in comparison with the benchmark Pt/C (0.095 A $mg_{Pt}^{-1}$) at 0.8 V, which was almost 21 times higher than the corresponding value of Pt/C. It evinces the superb ORR intrinsic catalytic activity of the as-prepared composite catalysts by the beneficial synergistic effect even though a very small amount of Pt/C was mixed well with $LiCoO_2$. Besides, the Tafel slope was adopted as another figure of merit. As can be seen in Fig. 2f, the excellent catalytic activity for the ORR on the composite electrodes was further proved by the smaller slopes of Tafel plots with the values of 55, 55 and 61 mV dec$^{-1}$ for Pt–$LiCoO_2$ (1 : 9, 1 : 19 and 1 : 49) composites, respectively, than that of Pt/C (69 mV dec$^{-1}$), again suggesting faster ORR kinetics of the composite samples.

The RRDE technique is extremely effective in evaluating the catalytic activity of electrocatalysts for the ORR by directly monitoring the generation rate of $HO_2^-$ during the ORR. We also adopted this technique to further verify the ORR pathway on the prepared composite catalyst. Fig. 3a shows the current on the disk electrode ($I_d$) and the ring electrode ($I_r$, multiplied by 100) using the Pt–$LiCoO_2$ (1 : 49) catalyst at various rotation speeds. Obviously, the $I_d$ was far higher than $I_r$, suggesting that a small amount of $HO_2^-$ was produced during the ORR process. As illustrated in Fig. 3b, the amount of formed $HO_2^-$ was less than 4% and the value of $n$ was above 3.92 for the Pt–$LiCoO_2$ (1 : 49) catalyst over a wide potential range from 0.35 to 0.85 V at all the rotating rates. It is consistent with the results obtained from the fitted K–L plot, which denotes a 4e$^-$ ORR process.

Table 1 Assessment of bifunctionality of Pt/C, Pt–$LiCoO_2$ composites with different mass ratios, $LiCoO_2$ and other catalysts reported in the literature in 0.1 M KOH solution at a rotation rate of 1600 rpm

| Sample | ORR $E$ @ −3 mA $cm^{-2}$ (V) | OER $E$ @ 10 mA $cm^{-2}$ (V) | $\Delta E$ (V) | Catalyst loading (mg $cm^{-2}_{disk}$) |
|---|---|---|---|---|
| 20 wt% Pt/C | 0.84 *vs.* RHE | 1.83 *vs.* RHE | 0.99 | 0.065 |
| Pt–$LiCoO_2$ (1 : 9) | 0.81 *vs.* RHE | 1.67 *vs.* RHE | 0.86 | 0.065 |
| Pt–$LiCoO_2$ (1 : 19) | 0.80 *vs.* RHE | 1.67 *vs.* RHE | 0.87 | 0.065 |
| Pt–$LiCoO_2$ (1 : 49) | 0.79 *vs.* RHE | 1.70 *vs.* RHE | 0.91 | 0.065 |
| $LiCoO_2$ | 0.56 *vs.* RHE | 1.71 *vs.* RHE | 1.15 | 0.065 |
| Pt/C to BSCF/C = 1 : 4 (ref. 45) | 0.76 *vs.* RHE | 1.59 *vs.* RHE | 0.83 | $0.26_{ORR}$ $0.19_{OER}$ |
| LT-$LiCoO_2$ (ref. 33)[a] | ~0.55 *vs.* RHE | ~1.70 *vs.* RHE | 1.15 | 0.25 |
| H–Pt/$CaMnO_3$ (ref. 37) | — | — | 1.01 | 0.085 |
| 20 wt% Ir/C (ref. 55) | 0.69 *vs.* RHE | 1.61 *vs.* RHE | 0.92 | 0.028 |
| 20 wt% Ru/C (ref. 55) | 0.61 *vs.* RHE | 1.62 *vs.* RHE | 1.01 | 0.028 |
| Mn oxide (ref. 55) | 0.73 *vs.* RHE | 1.77 *vs.* RHE | 1.04 | — |
| $LaNiO_{3-\delta}$ (ref. 58) | −0.32 *vs.* Ag/AgCl | ~0.71 *vs.* Ag/AgCl | 1.03 | 0.26 |
| $La_{0.3}(Ba_{0.5}Sr_{0.5})_{0.7}Co_{0.8}Fe_{0.2}O_{3-\delta}$ (ref. 59) | ~−0.32 *vs.* Hg/HgO | ~0.68 *vs.* Hg/HgO | 1.00 | 0.64 |
| $Fe_3O_4$/graphene (ref. 60) | ~0.6 *vs.* RHE | 1.78 *vs.* RHE | 1.18 | 0.20 |
| $MnCoFeO_4$/N-rGO (ref. 61)[a] | 0.78 *vs.* RHE | 1.71 *vs.* RHE | 0.93 | 0.10 |
| $La(Co_{0.55}Mn_{0.45})_{0.99}O_{3-\delta}$/N-rGO (ref. 62)[a] | ~−0.18 *vs.* Ag/AgCl | ~0.78 *vs.* Ag/AgCl | 0.96 | 0.25 |
| α-$MnO_2$ (ref. 63) | 0.76 *vs.* RHE | 1.72 *vs.* RHE | 0.96 | 0.20 |
| PCN on CFP (ref. 64)[a] | ~0.67 *vs.* RHE | 1.63 *vs.* RHE | 0.96 | 0.20 |

[a] LT = low temperature; N-rGO = nitrogen-doped reduced graphene oxide; PCN = phosphorus-doped g-$C_3N_4$; CFP = carbon-fiber paper.

Compared with Pt/C ($n$ > 3.94 and the amount of formed $HO_2^-$ < 2.91%) and pristine $LiCoO_2$ ($n$ > 3.80 and the amount of formed $HO_2^-$ < 9.96%) as shown in Fig. S5 of the ESI,† we found that the value of $n$ and the generation rate of $HO_2^-$ on the Pt–$LiCoO_2$ (1 : 49) catalyst was quite close to the results obtained on commercial Pt/C and superior to $LiCoO_2$, again indicating the much enhanced electrocatalytic efficiency due to the synergistic effect between Pt and $LiCoO_2$.

Besides the high ORR catalytic activity that is comparable to that of Pt/C, the Pt–$LiCoO_2$ (1 : 49) also exhibited a strong durability superior to Pt/C in the potential range of the ORR. For instance, the retention of the current was still up to 97.5% for the newly developed composite catalyst of Pt–$LiCoO_2$ (1 : 49) after the continuous polarization period of 10 h (Fig. 4a). In contrast, a significant attenuation with the loss of 13.8% of the initial current was observed for the Pt/C catalyst under the same operating conditions. Additionally, the methanol tolerance is also a significant index for the cathode materials of direct-methanol fuel cells (DMFCs). As shown in Fig. 4b, the initial cathodic current for the ORR on the commercial Pt/C electrode suddenly shifted to a reverse anodic current upon the addition of methanol, suggesting the conversion of the dominated process from the ORR to the methanol oxidation reaction. It demonstrates the poor ability of the Pt/C catalyst to resist the poisoning cross-over effects. With the reduction of the platinum content in the composite electrocatalysts, the cross-over effect was gradually suppressed. Especially for the Pt–$LiCoO_2$ (1 : 49) catalyst, only a slight change was observed after the introduction of methanol into the electrolyte, indicating its high selectivity for the ORR in a methanol-containing environment. LSV curves before and after adding methanol were very similar (Fig. S6†), further proving that the Pt–$LiCoO_2$ (1 : 49) catalyst possesses excellent tolerance to methanol, thus being a promising electrode material in DMFCs.

## Electrochemical behaviour for OER

The electrocatalytic activity of the as-prepared composite catalysts for the OER was investigated by extending the potential window to the water oxidation range. Typical LSV curves are shown in Fig. 5a for Pt–$LiCoO_2$ composites, and Pt/C and $LiCoO_2$ catalysts at 1600 rpm. All the composite catalysts afforded higher OER current than either pristine $LiCoO_2$ or Pt/C, suggesting their improved catalytic performances toward the OER. It is meaningful to compare the overpotential ($\eta$) for achieving a current density of 10 mA $cm^{-2}$, which is a metric standard relevant to solar fuel synthesis.[55] As shown in Fig. 5a, the values of $\eta$ were calculated to be 0.60, 0.44, 0.44, 0.47 and 0.48 V for Pt/C, Pt–$LiCoO_2$ (1 : 9, 1 : 19 and 1 : 49) and pristine $LiCoO_2$ respectively based on the standard potential for the electrolysis of water to oxygen being 1.23 V. Our composite catalysts rendered small values of $\eta$, especially for Pt–$LiCoO_2$ (1 : 9) and (1 : 19), showing the lowest $\eta$ with the value of 0.44 V among all the tested catalysts. The OER kinetics of electrocatalysts were estimated by comparing the slopes of the corresponding Tafel plots. As can be seen in Fig. 5b, the smallest Tafel slope of 82 mV $dec^{-1}$ was achieved for the Pt–$LiCoO_2$ (1 : 19) catalyst, whereas the pristine $LiCoO_2$ showed a higher value of 89 mV $dec^{-1}$, similar to the reported value in the literature.[56] These results clearly demonstrated that the composite catalysts possess high OER catalytic activity. The stability of the catalysts in the alkaline electrolyte was explored by carrying out 50 continuous potential cycles on the RDE at a rotation rate of 1600 rpm (Fig. S7 of the ESI†). The attenuation of the maximum current density within the tested potential

 

range was 25% for the pristine $LiCoO_2$ electrode after 50 cycles, while the current on the Pt–$LiCoO_2$ (1 : 49) electrode decreased by 14% under the same conditions. It most likely results from the interaction between Pt and $LiCoO_2$, even though only a slight amount of Pt existed in the composite.

### Bifunctional activity assessment

Finally, the overall oxygen electrocatalytic activity of the as-prepared composite catalysts is summarized in Fig. 6. To evaluate the bifunctional activity of the catalysts, the potential difference between the ORR and OER is a common indicator, defined as $\Delta E = E_{OER}$ @ 10 mA $cm^{-2} - E_{ORR}$ @ −3 mA $cm^{-2}$. It is noteworthy that an ORR current density of −3 mA $cm^{-2}$ is around the half-wave potential of the state-of-the-art Pt/C catalyst, while an OER current density of 10 mA $cm^{-2}$ is almost equivalent to that of an ideal solar cell device with 10% efficiency.[57] The smaller difference in the potential values indicates the better bifunctional activity of the catalyst. Table 1 lists the values of $\Delta E$ of our catalysts and other reported state-of-the-art bifunctional catalysts in 0.1 M KOH solution at a rotation rate of 1600 rpm. The $\Delta E$ values were 0.86, 0.87 and 0.91 V for Pt–$LiCoO_2$ (1 : 9, 1 : 19 and 1 : 49) catalysts, respectively. Remarkably, these values fall into the lowest $\Delta E$ observed for all the excellent electrocatalysts in Table 1, only slightly higher than that of the Pt/C to BSCF/C catalyst = 1 : 4 (0.83 V), the best catalyst listed in Table 1. It should be noted that both the catalyst loading and the Pt content of our catalysts were lower than those of Pt/C to BSCF/C = 1 : 4. These are the possible reasons that resulted in the slightly lower bifunctionality of our electrocatalysts. Regardless, the as-prepared Pt–$LiCoO_2$ composite catalysts prepared by the simple ultrasonic mixing rendered superb bifunctional activity for the ORR and OER. It suggests that the as-prepared composites could be the optimal bifunctional catalysts. As mentioned above, the high bifunctionality of the series of Pt–$LiCoO_2$ composites could result from the synergistic effect between Pt and $LiCoO_2$, achieved by the alteration of the electronic structure of Pt on the one hand, and by the modification of the adsorption/desorption behaviours of oxygen-containing species.

## Conclusions

In summary, active and stable bifunctional electrocatalysts for the ORR and OER were successfully fabricated *via* simply ultrasonic mixing Pt/C with $LiCoO_2$. The Pt–$LiCoO_2$ (1 : 49) catalyst with an ultralow Pt content of 2 wt% exhibited an ORR catalytic activity comparable to that of commercial Pt/C with a Pt content of 20 wt%. Notably, a super high ORR mass activity of 2.04 A $mg_{Pt}^{-1}$ at 0.8 V was achieved for the Pt–$LiCoO_2$ (1 : 49) catalyst, which was 21-fold higher than that of Pt/C. Meanwhile, the as-prepared composite catalyst also exhibited favourable OER activity with a lower overpotential and Tafel slope. Good stability and methanol tolerance for the ORR and OER were demonstrated from the composite catalysts in this study. The outstanding electrocatalytic activity could arise from the interaction between Pt/C and $LiCoO_2$, which synergistically enhanced the bifunctionality of catalysts. The proposed simple method for preparing electrocatalysts with bifunctionality is a promising route to prepare practical Pt-based electrocatalysts with ultralow noble metal content, furthermore reducing the cost of electrochemical energy systems. The facile synthesis method and the effective performance enable our catalysts to be competitive candidates as the oxygen electrode of new energy devices, such as regenerative fuel cells and rechargeable metal–air batteries. Moreover, the present synthetic strategy can be generalized to produce highly active bifunctional catalysts by combining other ORR and OER catalysts with lower cost and higher activity.

## Acknowledgements

The work was supported by the Australian Research Council Discovery Project grant DP160104835. Dr Chao Su acknowledges Curtin University for a postdoctoral fellowship. Dr Tao Yang acknowledges the FCT for financial support *via* the grant SFRH/BPD/86336/2012. The authors also acknowledge the use of equipment, scientific and technical assistance of the WA X-Ray Surface Analysis Facility, funded by the Australian Research Council LIEF grant LE120100026.

## Notes and references

1 L. Li, Z. Wu, S. Yuan and X. B. Zhang, *Energy Environ. Sci.*, 2014, **7**, 2101.
2 M. K. Debe, *Nature*, 2012, **486**, 43.
3 J. S. Lee, S. T. Kim, R. Cao, N. S. Choi, M. Liu, K. T. Lee and J. Cho, *Adv. Energy Mater.*, 2011, **1**, 34.
4 T. Ogasawara, A. Débart, M. Holzapfel, P. Novák and P. G. Bruce, *J. Am. Chem. Soc.*, 2006, **128**, 1390.
5 G. Chen, S. R. Bare and T. E. Mallouk, *J. Electrochem. Soc.*, 2002, **149**, A1092.
6 B. D. McCloskey, D. S. Bethune, R. M. Shelby, T. Mori, R. Scheffler, A. Speidel, M. Sherwood and A. C. Luntz, *J. Phys. Chem. Lett.*, 2012, **3**, 3043.
7 A. A. Gewirth and M. S. Thorum, *Inorg. Chem.*, 2010, **49**, 3557.
8 E. Mirzakulova, R. Khatmullin, J. Walpita, T. Corrigan, N. M. Vargas-Barbosa, S. Vyas, S. Oottikkal, S. F. Manzer, C. M. Hadad and K. D. Glusac, *Nat. Chem.*, 2012, **4**, 794.
9 S. Park, Y. Shao, J. Liu and Y. Wang, *Energy Environ. Sci.*, 2012, **5**, 9331.
10 F. Cheng, J. Shen, B. Peng, Y. Pan, Z. Tao and J. Chen, *Nat. Chem.*, 2011, **3**, 79.
11 A. Indra, P. W. Menezes, N. R. Sahraie, A. Bergmann, C. Das, M. Tallarida, D. Schmeißer, P. Strasser and M. Driess, *J. Am. Chem. Soc.*, 2014, **136**, 17530.
12 Y. J. Sa, K. Kwon, J. Y. Cheon, F. Kleitzc and S. H. Joo, *J. Mater. Chem. A*, 2013, **1**, 9992.
13 T. Y. Ma, S. Dai, M. Jaroniec and S. Z. Qiao, *J. Am. Chem. Soc.*, 2014, **136**, 13925.
14 D. Wang, H. L. Xin, R. Hovden, H. Wang, Y. Yu, D. A. Muller, F. J. DiSalvo and H. D. Abruña, *Nat. Mater.*, 2013, **12**, 81.
15 J. W. Hong, S. W. Kang, B. S. Choi, D. Kim, S. B. Lee and S. W. Han, *ACS Nano*, 2012, **6**, 2410.

16 S. Hu, G. Goenaga, C. Melton, T. A. Zawodzinski and D. Mukherjee, *Appl. Catal., B*, 2016, **182**, 286.
17 Z. Li, Y. Li, S. P. Jiang, G. He and P. K. Shen, *J. Mater. Chem. A*, 2014, **2**, 16898.
18 S. Siracusano, N. V. Dijk, E. Payne-Johnson, V. Baglio and A. S. Aricò, *Appl. Catal., B*, 2015, **164**, 488.
19 R. Cao, W. Lai and P. Du, *Energy Environ. Sci.*, 2012, **5**, 8134.
20 K. L. Nardi, N. Yang, C. F. Dickens, A. L. Strickler and S. F. Bent, *Adv. Energy Mater.*, 2015, **5**, 1500412.
21 M. Orlandi, S. Caramori, F. Ronconi, C. A. Bignozzi, Z. E. Koura, N. Bazzanella, L. Meda and A. Miotello, *ACS Appl. Mater. Interfaces*, 2014, **6**, 6186.
22 Y. Zhu, W. Zhou, Z. G. Chen, Y. Chen, C. Su, M. O. Tadé and Z. Shao, *Angew. Chem., Int. Ed.*, 2015, **54**, 3897.
23 X. Xu, C. Su, W. Zhou, Y. Zhu, Y. Chen and Z. Shao, *Adv. Sci.*, 2016, **3**, 1500187, DOI: 10.1002/advs.201500187.
24 C. Su, W. Wang, Y. Chen, G. Yang, X. Xu, M. O. Tadé and Z. Shao, *ACS Appl. Mater. Interfaces*, 2015, **7**, 17663.
25 R. Liu, F. Liang, W. Zhou, Y. Yang and Z. Zhu, *Nano Energy*, 2015, **12**, 115.
26 J. Y. C. Chen, J. T. Miller, J. B. Gerken and S. S. Stahl, *Energy Environ. Sci.*, 2014, **7**, 1382.
27 X. Yu, Z. Sun, Z. Yan, B. Xiang, X. Liu and P. Du, *J. Mater. Chem. A*, 2014, **2**, 20823.
28 J. B. Goodenough and Y. Kim, *Chem. Mater.*, 2010, **22**, 587.
29 G. Gardner, J. Al-Sharab, N. Danilovic, Y. B. Go, K. Ayers, M. Greenblatt and G. C. Dismukes, *Energy Environ. Sci.*, 2016, **9**, 184.
30 S. W. Lee, C. Carlton, M. Risch, Y. Surendranath, S. Chen, S. Furutsuki, A. Yamada, D. G. Nocera and Y. Shao-Horn, *J. Am. Chem. Soc.*, 2012, **134**, 16959.
31 Z. Lu, H. Wang, D. Kong, K. Yan, P. C. Hsu, G. Zheng, H. Yao, Z. Liang, X. Sun and Y. Cui, *Nat. Commun.*, 2014, **5**, 4345, DOI: 10.1038/ncomms5345.
32 N. Colligan, V. Augustyn and A. Manthiram, *J. Phys. Chem. C*, 2015, **119**, 2335.
33 T. Maiyalagan, K. A. Jarvis, S. Therese, P. J. Ferreira and A. Manthiram, *Nat. Commun.*, 2014, **5**, 3949, DOI: 10.1038/ncomms4949.
34 B. Han, D. Qian, M. Risch, H. Chen, M. Chi, Y. S. Meng and Y. Shao-Horn, *J. Phys. Chem. Lett.*, 2015, **6**, 1357.
35 J. M. Jaksic, D. Labou, G. D. Papakonstantinou, A. Siokou and M. M. Jaksic, *J. Phys. Chem. C*, 2010, **114**, 18298.
36 V. T. T. Ho, C. J. Pan, J. Rick, W. N. Su and B. J. Hwang, *J. Am. Chem. Soc.*, 2011, **133**, 11716.
37 X. Han, F. Cheng, T. Zhang, J. Yang, Y. Hu and J. Chen, *Adv. Mater.*, 2014, **26**, 2047.
38 Z. Awaludin, M. Suzuki, J. Masud, T. Okajima and T. Ohsaka, *J. Phys. Chem. C*, 2011, **115**, 25557.
39 Y. Liang, Y. Li, H. Wang, J. Zhou, J. Wang, T. Regier and H. Dai, *Nat. Mater.*, 2011, **10**, 780.
40 S. Mao, Z. Wen, T. Huang, Y. Hou and J. Chen, *Energy Environ. Sci.*, 2014, **7**, 609.
41 S. Liu, W. Bian, Z. Yang, J. Tian, C. Jin, M. Shen, Z. Zhou and R. Yang, *J. Mater. Chem. A*, 2014, **2**, 18012.
42 D. U. Lee, H. W. Park, M. G. Park, V. Ismayilov and Z. Chen, *ACS Appl. Mater. Interfaces*, 2015, **7**, 902.
43 H. Wang, Y. Yang, Y. Liang, G. Zheng, Y. Li, Y. Cui and H. Dai, *Energy Environ. Sci.*, 2012, **5**, 7931.
44 Y. Gao, H. Zhao, D. Chen, C. Chen and F. Ciucci, *Carbon*, 2015, **94**, 1028.
45 Y. Zhu, C. Su, X. Xu, W. Zhou, R. Ran and Z. Shao, *Chem.–Eur. J.*, 2014, **20**, 15533.
46 J. Sunarso, A. A. J. Torriero, W. Zhou, P. C. Howlett and M. Forsyth, *J. Phys. Chem. C*, 2012, **116**, 5827.
47 C. A. Hancock, A. L. Ong, P. R. Slater and J. R. Varcoe, *J. Mater. Chem. A*, 2014, **2**, 3047.
48 S. Jeong, S. Park and J. Cho, *Adv. Energy Mater.*, 2011, **1**, 368.
49 D. Qian, Y. Hinuma, H. Chen, L. S. Du, K. J. Carroll, G. Ceder, C. P. Grey and Y. S. Meng, *J. Am. Chem. Soc.*, 2012, **134**, 6096.
50 Y. Zhao, Y. Sha, Q. Lin, Y. Zhong, M. O. Tadé and Z. Shao, *ACS Appl. Mater. Interfaces*, 2015, **7**, 1787.
51 L. Dahéron, R. Dedryvère, H. Martinez, M. Ménétrier, C. Denage, C. Delmas and D. Gonbeau, *Chem. Mater.*, 2008, **20**, 583.
52 N. H. Chou, P. N. Ross, A. T. Bell and T. D. Tilley, *ChemSusChem*, 2011, **4**, 1566.
53 B. S. Yeo and A. T. Bell, *J. Am. Chem. Soc.*, 2011, **133**, 5587.
54 H. Liao and Y. Hou, *Chem. Mater.*, 2013, **25**, 457.
55 Y. Gorlin and T. F. Jaramillo, *J. Am. Chem. Soc.*, 2010, **132**, 13612.
56 Y. Zhu, W. Zhou, Y. Chen, J. Yu, M. Liu and Z. Shao, *Adv. Mater.*, 2015, **27**, 7150.
57 D. Chen, C. Chen, Z. M. Baiyee, Z. Shao and F. Ciucci, *Chem. Rev.*, 2015, **115**, 9869.
58 W. Zhou and J. Sunarso, *J. Phys. Chem. Lett.*, 2013, **4**, 2982.
59 J. I. Jung, H. Y. Jeong, J. S. Lee, M. G. Kim and J. Cho, *Angew. Chem., Int. Ed.*, 2014, **53**, 4582.
60 B. Zhao, Y. Zheng, F. Ye, X. Deng, X. Xu, M. Liu and Z. Shao, *ACS Appl. Mater. Interfaces*, 2015, **7**, 14446.
61 Y. Zhan, C. Xu, M. Lu, Z. Liu and J. Y. Lee, *J. Mater. Chem. A*, 2014, **2**, 16217.
62 X. Ge, F. W. T. Goh, B. Li, T. S. A. Hor, J. Zhang, P. Xiao, X. Wang, Y. Zong and Z. Liu, *Nanoscale*, 2015, **7**, 9046.
63 Y. Meng, W. Song, H. Huang, Z. Ren, S. Y. Chen and S. L. Suib, *J. Am. Chem. Soc.*, 2014, **136**, 11452.
64 T. Y. Ma, J. Ran, S. Dai, M. Jaroniec and S. Z. Qiao, *Angew. Chem., Int. Ed.*, 2015, **54**, 4646.